The Pennsylvania State University

Wind Energy Club

Technical Design Report

Submitted to the 2023 U.S. Department of Energy Collegiate Wind Competition
May 4, 2023

Aerodynamic Design Team

Shana Hartwick	**Director**
Alex Scheffler-Murry	**Lead**
Austin DiSciullo	**Lead**
Diana Deleon	Member
Jue Huang	Member
Lauren Myers	Member
Jason Oh	Member
Daniel Romero	Member
Kathryn Sharp	Member
Rochelle Xavier	Member

Generator Design Team

Conner Burger	**Director, VP**
Kan Petyim	Member
Armend Berisha	Member
Ryan Manning	Member
Aditya Ghadigaonkar	Member
Luke Price	Member

Foundation Design Team

Eric Sarbacker	**Director**
Matthew Reagan	Member
Liam Cassidy	Member

Electrical Design Team

Satyam Patel	**President**
Rahul Shekar	**Co-Lead**
Hamdan Almarzooqi	**Co-Lead**
Alan Arechiga	Member
Caroline Brustoloni	Member
Ethan Farrow	Member
CJ Young	Member
Anum Jan	Member
Ian Lin	Member
Folayemi Omogboyega	Member
Blake Wall	Member
Erik Long	Member
Maddi Waehner	Member
Megan Wolff	Member

Software Design Team

Brian Truong	**Director**
Jiaming Wang	**Lead**
Mark Young	Member
Parth Kshirsagar	Member
Yashas Anapindi	Member

Academic Advisors

Dr. Susan W. Stewart
Dr. Mark A. Miller

COLLEGIATE WIND COMPETITION
U.S. DEPARTMENT OF ENERGY

Table of Contents

ABSTRACT

This report outlines the design of a fixed-bottom offshore wind turbine developed by the Penn State Wind Energy Club for the 2023 Collegiate Wind Competition. The team had maintained a conservative approach to design changes from the 2019 to 2022 competition year - focusing on incremental improvements to inadequate subsystems while maintaining other systems at satisfactory level. However, following lackluster performance in the 2022 competition, the team has completely overhauled the wind turbine for the 2023 competition. This newly designed wind turbine is shown in Figure 1, and Figure 2.

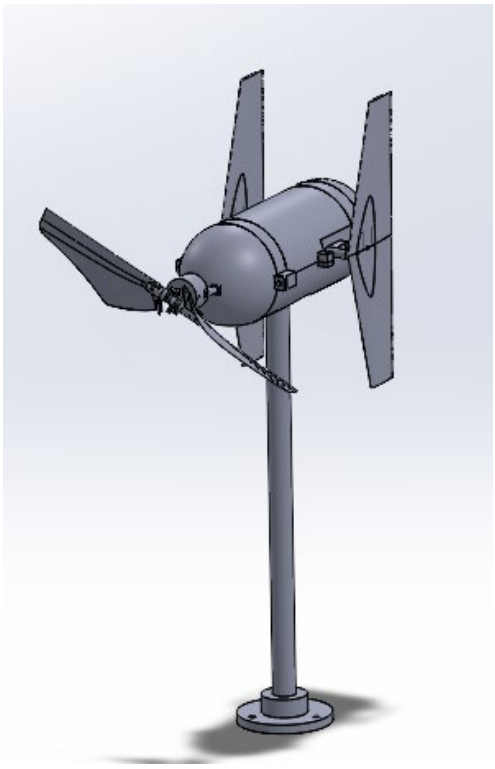

Figure 1 CAD Rendering of the Assembled Turbine

The primary design objective was to redesign every subsystem of the turbine focusing on safety, reliability, and efficiency. The turbine is composed of five subsystems: aerodynamics, generator, foundation, electronics, and software. In redesigning each subsystem, the team reviewed the weak points of previous iterations while developing new ideas around the 2023 rules and regulations.

Figure 2 Assembled Turbine

The turbine utilizes a two-blade rotor to operate the nine-phase, three-stage axial flux permanent magnet generator. The nacelle encloses the generator, and it follows a “soda bottle” shape to house two linear actuators that operate the pitching mechanism. The nacelle also encloses an onboard rectifier to convert AC power produced by the generator directly to DC. A hall effect sensor is embedded within the generator to monitor turbine RPM. In addition, a pitot tube pressure differential sensor is also mounted to measure airspeed.

A turbine-side power-and signal modulation box is used to regulate power produced by the turbine to operate all the turbine peripherals. Power produced by the turbine is across the Point of Common-Coupling (PCC) where it is consumed by the 10 Ω – 160 Ω variable load. Two microcontrollers are housed in the load box which operates the control code that operates the wind turbine. The control system can shut down the turbine when it detects a PCC disconnect, or when the Emergency Stop button is depressed. The control also runs various algorithms that manipulate pitch angle and load resistance depending on the operational state.

AERODYNAMICS DESIGN

The aerodynamic subsystem's design objective was primarily focused on streamlining the turbine nacelle while improving the component packaging and improving overall reliability and performance. While the two bladed designs have remained the same this year, nearly all other components of the nacelle and blades have been either updated or remanufactured using new materials.

Blade Design, Manufacturing, & Analysis

The design of the blades attempted to optimize the rotor power output while considering the small scale of the competition rotor. Since the blade radius was constrained to 45-cm, the rotor aerodynamics are quite different than large, commercial wind turbines. The rotor's design goal was to maximize the glide ratio, or ratio of lift to drag forces, $\frac{C_l}{C_d}$. The airfoil chosen to achieve this is the Ma 409, shown in Figure 3. Drag generally decreases and the stall point of an airfoil increases as the scale or Reynolds number, Re, of an airfoil becomes larger. Increasing the Re is most easily accomplished by increasing the chord length along the rotor blade. However, only increasing chord length causes the rotor solidity, or ratio of blade area to rotor swept area, to increase as well. This has the effect of reducing the point of maximum rotor efficiency in the power coefficient, $C_{p,max}$onsequently, the aerodynamics team reduced the number of blades from three to two in order to keep the rotor solidity approximately constant.

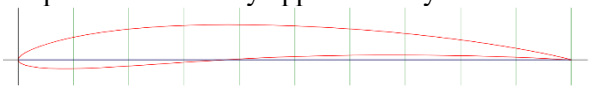

Figure 3 Ma 409 airfoil.

This year the Aerodynamics team focused on fixing structural and integration challenges from prior years instead of redesigning the aerodynamic shape of the blades. One aspect of this was identifying a stronger blade material. Figure 4 shows three blades—moving from left to right—from 2021, 2022, and 2023, respectively. The 2021 blade was made of Nylon 12. The Nylon 12 blades not as rigid as expected, primarily due to issues with the blade CAD model which was fixed in later years. The 2022 blade was fabricated using Accura 60 and an updated CAD model, making for a blade with much higher stiffness. The Accura 60 blades had a smoother surface finish due to the stereolithography 3D printing process used to fabricate them. The Accura 60 blades were however very brittle near the trailing edge, which made transportation and handling difficult. Online fabrication service Xometry manufactured both the Nylon 12 and Accura 60 blades. The 2023 blades were fabricated using a different stereolithographic 3D printing material called Rigid 10K, and were fabricated by the Penn State Applied Research Laboratory (ARL). ARL recommended Rigid 10K because they often print research-quality rotorcraft blades with the material. The team ultimately chose Rigid 10K because of the material's stiffness. Rigid 10K can withstand significant loads without bending [1]. Wind turbine blade stiffness is important because blade deformation can cause an unstable power output [2].

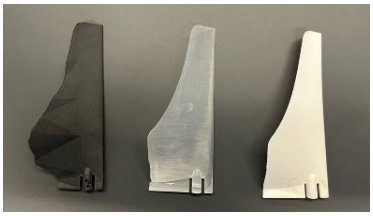

Figure 4 Blade evolution from left to right.

To validate the blade material choice, the team conducted a finite element analysis (FEA) on blade geometries using Rigid 10K's material properties from the manufacturer (Formlabs) in SOLIDWORKS, using the von Mises stress criterion to map the stress levels. The FEA was then compared to past FEA for Nylon 12 and Accura 60. The figures below represent the FEA results, with warmer colors indicating higher stress (red highest) and cooler color indicating lower stress (blue lowest).

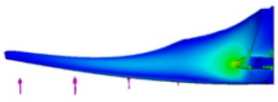

Figure 5 Stress results for Nylon 12

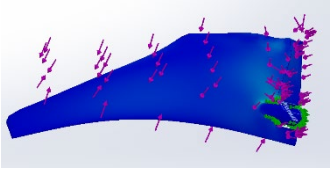

Figure 6 Stress results for Accura 60

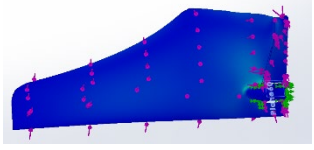

Figure 7 Stress results for Rigid 10K

The FEA results indicate that Rigid 10K experiences lower peak stress as compared to Nylon 12. In Figure 5, there is a point of high stress near the root, which is indicated in green. In comparison, the FEA using Rigid 10K, shown in Figure 7, experiences less stress at the same region due to lower deflections and greater stiffness. When comparing the Accura 60 and Rigid 10K (Figures 6 and 7), the amount of stress experienced appears relatively similar. However, the stress results show a larger deflection for Accura 60 as compared to Rigid 10K. The estimated deflection value for the Accura 60 was 58.27 mm compared to Rigid 10K's lower 17.52 mm. To investigate the blade deflections further, another SOLIDWORKS simulation was created where different loads were applied to determine the tip deflection.

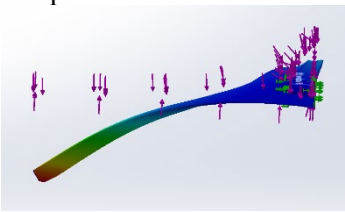

Figure 8 Deflection results for Accura 60

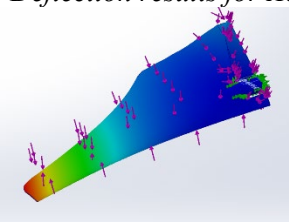

Figure 9 Deflection results for Rigid 10K

Figures 8 and 9 suggest that the Accura 60 experiences a larger deflection than Rigid 10K. An experimental test was conducted to confirm this simulation result. The blade deflection test was conducted by sliding a clamp onto the blade. The blade was weight applied at the midspan because the team had 3-D printed clamping blocks to use at this location. The clamp had a hook to which loads could be applied. The hook was loaded in 8.896-N increments until the total weight equaled 31.138-N which was the maximum that could be applied with this method.

Figure 10 verifies the SOLIDWORKS simulation. The Accura 60 material experiences more deflection than the Rigid 10K material. The culmination of the blade analysis supports the team's decision to proceed with Rigid 10K as the blades' final material.

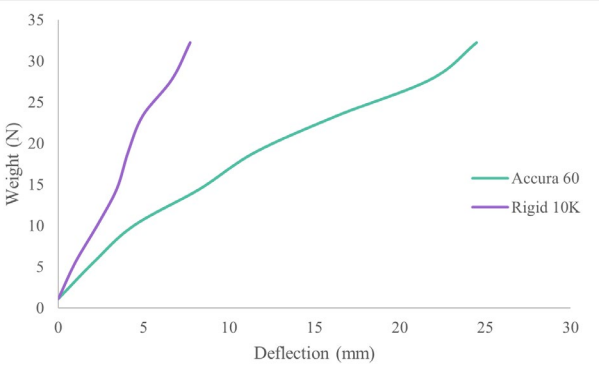

Figure 10 Weight versus deflection

Rotor Hub

The turbine uses an Align 700 rotor hub—a repurposed RC helicopter tail rotor. The rotor hub was strength tested during the 2021 competition year. To conduct the strength testing, a block with a rod on one end was clamped to an I-beam that was attached to a strongback on the wall of the Aerospace Engineering's structures lab. The rod emulated the drive shaft and the rotor hub was attached to it in the same way as the competition turbine. A bolt was then fixed to the rotor hub piece. A chain was attached to the bolt and applied an upward force on the rotor hub. The SolidWorks model estimated that the rotor hub should withstand an estimated 110 N on each side to fully support the blades at their maximum speed. The rotor hub was tested up to 890 N with only minimal damage to the screw, making the test successful with a safety factor of 8.09. Since the current rotor has not been damaged in the past two years, the team did not retest the rotor hub's strength due to its high factor of safety.

Collective Blade Pitch System

The rotor hub pitch mechanism is actuated by two parallel linear actuators to simultaneously pitch the blades. The previous pitch mechanism used six different pieces to connect the rotor and the linear actuators. The pitch mechanism—shown in Figure 11—was redesigned to use one circular cuff to connect the rotor and linear actuators. The linear actuators connect on either side of the circular cuff. Reducing the pitch mechanism from six pieces to one piece simplified the design while ensuring that the system does not create an undesirable bending moment when operating.

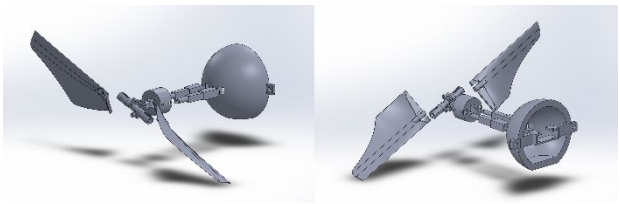

(a) Front *(b) Back*

Figure 11 Exploded View of Pitch System

Nacelle Design, Manufacturing, & Analysis

The past nacelle design included a rectangular body with a rounded lid, which resembled a mailbox. The nacelle was designed to *only* house the generator, leaving little room for electronics or other hardware. This year, the team decided to focus on completely redesigning the nacelle to create a more streamlined turbine shape and integrate the electronics and hardware in a more functional package.

The redesigned nacelle consists of four main components: the nosecone, midsection, lid, and tailcone, shown in Figure 12. Figure 13 shows a SOLIDWORKS flow visualization simulation, verifying that the new nacelle design is more streamlined than the mailbox-shaped nacelle.

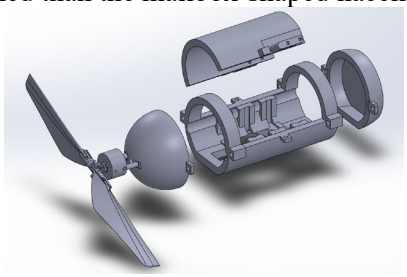

Figure 12 Exploded view of nacelle

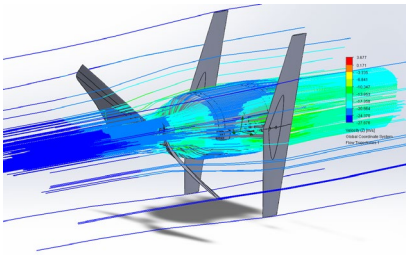

Figure 13 Flow visualization

A new design requires a new loading analysis. In a similar method to the blade analysis, SOLIDWORKS was used to model the forces that the nacelle will experience. Figure 14 shows that the nacelle sees the largest force at the front of the nosecone and at the leading edges of the tail fins. Because of the high forces generated on the nosecone of the nacelle, a simulation predicting the stresses that the nosecone will experience individually was generated and is presented in Figure 15.

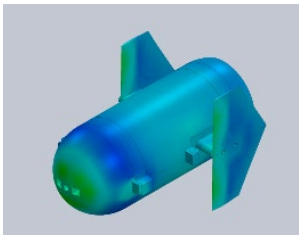

Figure 14 Pressure distribution

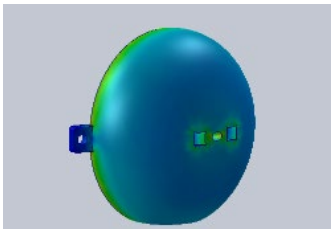

Figure 15 Stress Diagram for Nacelle Nose Cone

Figure 15 predicts that the highest areas of stress will be where the linear actuators for the pitching mechanism and the rotor axle turbine are located. To strengthen the nosecone and the rest of the nacelle, the nacelle's wall thickness was made to be 1.26-cm.

Passive Yaw System

The passive yaw system on the nacelle is much different than designs in prior years. Moving the linear actuators for the pitch mechanism inside the nacelle caused the nacelle's overall length to increase, leaving no room for a vertical stabilizer on the back of the nacelle. Mounting a fin on the top and bottom would limit the vertical stabilizer's length. Consequently, the new passive yaw system design includes two tailfins on either side of the nacelle lid, as shown in Figure 13. The tailfins are mounted as far back on the nacelle body as possible to maximize the restoring moment that the tailfins will exert as the turbine attempts to yaw during operation. Analysis of several symmetrical NACA series airfoils showed that the NACA-0009, shown in Figure 16, had several positive attributes including the greatest lift-curve slope of the symmetrical airfoils studied, the widest range of angles of attack before stall, and the smallest profile drag coefficient. Thus, the NACA-0009 is the most effective at producing a restoring moment to align the turbine with the oncoming wind and was chosen for the new tailfins.

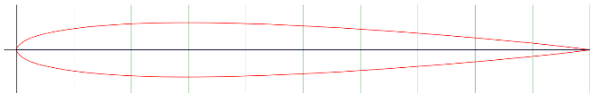

Figure 16 NACA-0009 airfoil

GENERATOR DESIGN

The generator converts mechanical energy produced by the blades into electrical energy. Electromagnetic generators translate rotational kinetic energy to a spinning rotor with embedded magnets or conductive coils. Permanent magnets produce magnetic fields with opposite directions on each face as illustrated in Figure 17. The north pole of a permanent magnet emits a positive magnetic field leaving the surface, and the south pole of a permanent magnet emits a negative magnetic field.

Due to the rotation, the magnetic flux passing through the conductive coils is continuously changing. As described by Faraday's Law (Eq.1), changes in magnetic flux will induce an EMF. Lenz's Law dictates that the induced current will produce a magnetic field in the opposite direction of the inducing magnetic field.

$$E_b = -N\left(\frac{d\Phi}{dt}\right) \quad (1)\ \textit{Lenz's Law}$$

There are two primary types of Electromagnetic Generator Designs: Axial Flux Generator [AFG], and Radial Flux Generator [RFG]. Magnetic flux changes in the direction parallel to the axis of rotation in an AFG. The magnetic flux changes in the direction perpendicular to the axis of rotation in an RFG as illustrated in Figure 17.

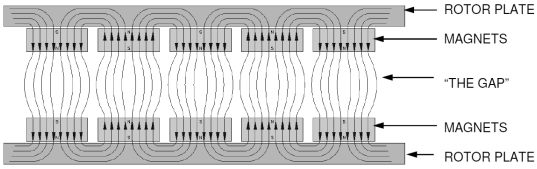

Figure 17: Flux Lines Traced Through an Axial Flux Dual-Rotor Permanent-Magnet Generator Source: Adapted from [5]

The team chose an axial flux design due to its manufacturability, adjustability, and efficiency. RFGs utilize enveloping cylinders to hold the stator and rotor in place. These parts can be difficult to fabricate through additive manufacturing; however, the disk stator and rotor designs of AFGs are much easier to produce with 3D printing. RFGs need new stator/rotors to adjust airgaps. The airgaps in AFGs can be adjusted by sliding the rotor/stator along the axle. The path of magnetic flux in an AFG is relatively short compared to the RFG, and therefore has a lower price to performance ratio in comparison to RFGs [6].

To design an axial flux generator, a major parameter to determine is the number of poles. Each magnet in the rotors creates a pole for the generator. To have an efficient generator a ratio of four poles to three stators coils must be maintained [6]. Our design specifically includes eight poles and six coils per stator. The AC output frequency of the generator is dependent on the turbine's rotational speed and number of poles as show in Eq. 2. However, since the output is rectified to DC the AC frequency is irrelevant.

The strength and dimensions of the magnets used also play a critical role in the electrical output of the generator. The magnets used are N52 grade cylindrical magnets with a diameter of 0.5 in and a height of 0.1875 in with a remnant magnetic field strength of 1.48 Tesla. The field strength reaching the surface of the stator is a strong function of air gap. The airgap is important since magnetic field strength decreases as the distance from the magnet increases as seen in Figure 17. Given the team's smallest achievable air gap of 1.8 mm the stator surface magnetic field strength is 4.296 Tesla.

The max magnetic flux is used to find the number of turns needed in each coil and is found by multiplying the surface magnetic field strength by the magnets' circular surface area as seen in Eq. 3. Eq. 4 shows the relationship between the number of coils and the generator parameters. Using this relationship, the team created a MATLAB calculator to determine the number of turns needed per coil to be 276.

Poles and Rotational Speed

$$P = \frac{120\, f_{nom}}{n_{nom}} \quad (2)$$

Flux Max from Magnetic Field Intensity

$$\phi_{max} = B_{mg} * A 3)$$

Number of Turns Calculation

$$N_c = \frac{\sqrt{2}E_f}{q*2\pi*\kappa_w\phi_{max}*n*\frac{p}{120}} 4)$$

Where:

E_f	electro-magnetic force (V)
k_w	$Winding\ Coefficient$ (0.95)
n	generator RPM
p	number of pole pairs
q	number of coils per phase

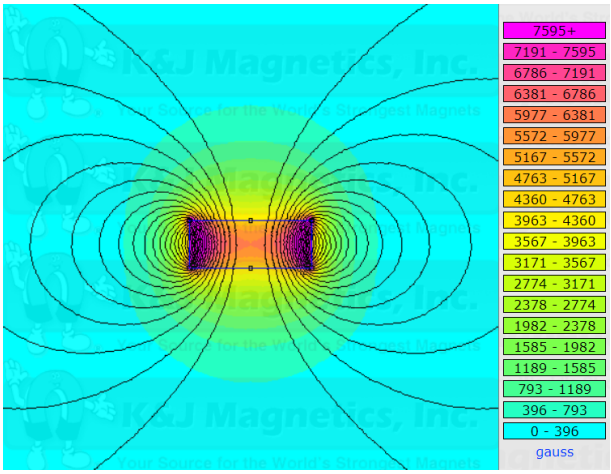

Figure 18 Magnetic Field Map of Magnets Used in Rotor Source: Adapted From [7]

The key features that needed improvement from last year's design are size, weight, and rotor clearances. To reduce size and weight the three generator stages were moved closer with virtually no gap between each stage which also allowed for the aluminum carriage to be shortened, reducing weight. To further reduce weight a much thinner carriage was used again replacing aluminum with the lighter 3D printed nacelle. To create better rotor clearances, new rotors with a smaller tolerance of the shaft hole were used to keep the rotors perpendicular to its surface. The final dimension was determined by 3D printing circular holes with various diameters and testing their fitment on the shaft. This allowed the team to achieve the 1.8 mm airgap described above. The final generator design is seen in Figure 19 and Figure 20.

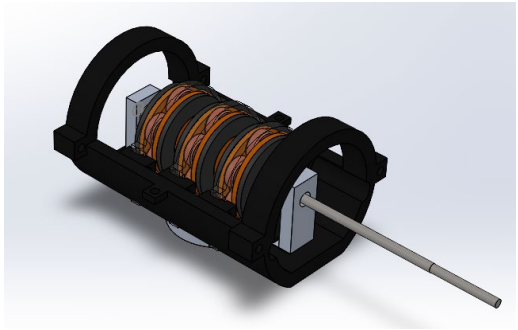

Figure 19 Generator SolidWorks

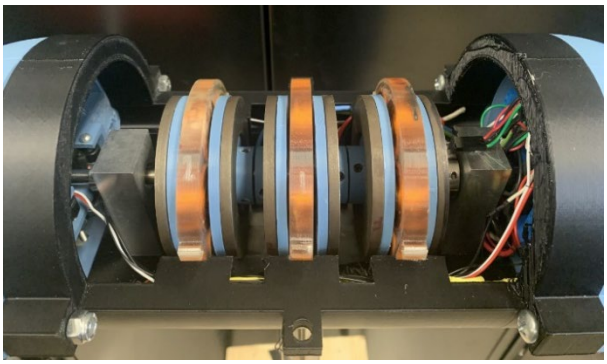

Figure 20 Physical Generator

Performance

To measure the generator's performance the team used a dynamometer and connected the generator's input shaft to the device. The dynamometer allows for the rpm to be changed while a variable load allows for various loading conditions to be tested. The team completed runs varying the rpm while keeping load constant for each run. The results of this testing are displayed in Figure 21. These results reveal that at lower loads more power is produced, but the higher loads allow for greater speeds. The team capped the testing speed at 2000 rpm since this rpm caused the dynamometer to reach its input power maximum. Comparing the results to last year's generator we find slight increases in power due to the smaller airgap. The generator also ran much smoother than the previous design with less vibration due to the tighter stator holders and rotor tolerances.

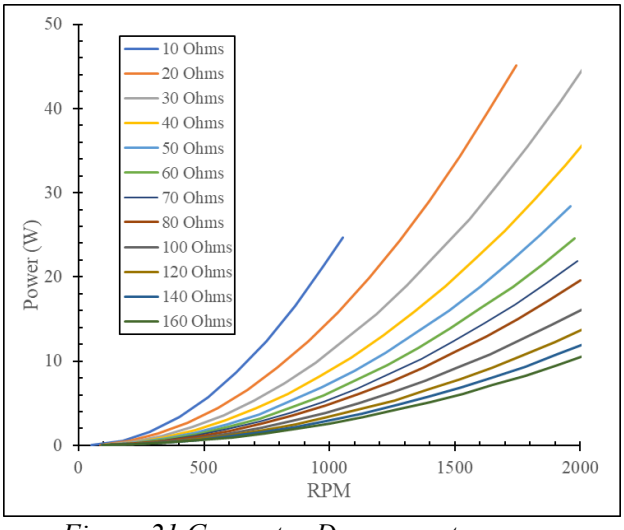

Figure 21 Generator Dynamometer Performance Curves

Foundation Design

The fixed offshore turbine foundation is the newest challenge to the Collegiate Wind Competition. The team discarded the previously attempted suction caisson design, and instead of researching other commercially used offshore foundations, gathered inspiration from previously successful foundations as they directly account for the same installation scenario. The most effective designs were similar to the suction caisson or used anchors.

The Sand Screw Egg Crate

The design for the foundation is based on egg crate paneling, which is commonly used in lighting. This design was chosen due to its ability to be easily designed, manufactured, and tested. The egg crate panels were designed such that there are two different configurations within the foundation, as shown in Figure 22. Typically, only configuration A would be necessary, but configuration B allows for two sides of the egg crate to support all adjoining sides. Thus, two configuration A panels were bolted to the top plate of the foundation, preventing any other paneling from falling out. Additionally, two B panels were bolted as well for stability and to maintain symmetry.

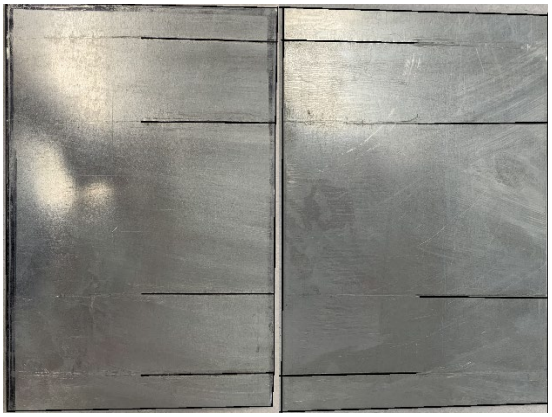

Figure 22 Egg crate panel configuration A (left) and B (right)

The foundation is critical to the turbine operation and must support all mechanical and aerodynamic loads imposed by the turbine system. This task was assessed by first understanding that the largest risk to the turbine's stability is the 11.5 lbs. of thrust force caused by the blades. Accounting for the 4 ft. moment arm from the top of the sand to the centerline of the turbine, the maximum load of the turbine is 46 ft-lbs. of torque can be expected at 25 m/s. As an added precaution against any time-dependent weakening of the foundation, the team decided on a safety factor of 2 for the moment resistant capacity.

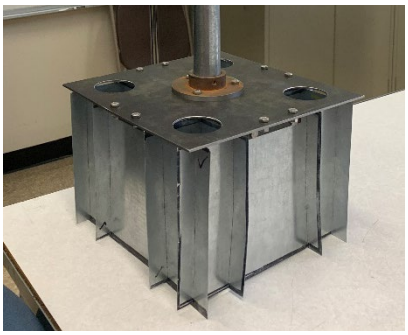

Figure 23 Fully Built Foundation

To retain the spirit of commercialized installation, the foundation design was developed such that it could be installed facing any direction and that the turbine could resist winds from any direction. The foundation is designed to hold four screws as this choice provides the aforementioned safety factor but could be modified slightly to account for more screws, and thus more stability to ensure safety during emergency scenarios that occur during high wind speeds.

Installation

The current foundation design prioritizes a fast installation time. First an orbital hand sander is used to vibrate the egg crate into the sand, then the anchors are drilled into the sand using an impact drill. The installation of the anchors adds additional resistance to tipping, but also aids in packing the sand within the foundation.

Testing

The foundation was tested in all aspects of operation for the competition: weight, installation, and durability. The weight of 5.2 kg was measured using a scale. Practiced installations of the foundation in a simulation sand box were done and total installation took on average: 10.42 minutes.

Durability was tested more thoroughly as it was considered the highest priority for the competition turbine. Experiments were done via a series of tip over tests to examine the capabilities of the foundation design, where a moment would be applied until the foundation failed. To apply a moment to the foundation, a weight was attached to a string that ran over a pulley and connected to a moment arm. Failure is determined either when the

tower shifted greater than 10mm or 15º. The test setup can be seen in Figure 24. Different combinations of anchors and walls were tested to empirically model the strength of the various configurations.

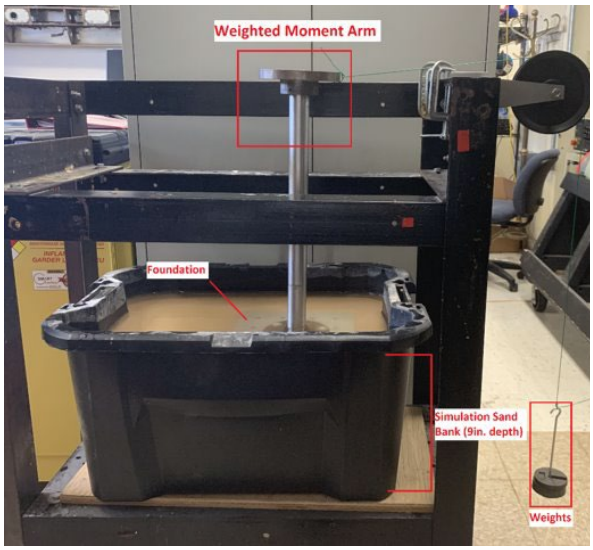

Figure 24 Foundation Testing Rig

The sole testing of anchors determined that the anchors near the tail of the turbine had little to no effect on the tip-over moment resistance of the foundation. The anchors were symmetric in strength fore and aft, perpendicular to the direction of wind, and their moment-resistive force can be described using Eq. 5.

$$R(x) = (R_{max} - R_{min})e^{\left(-\frac{\pi}{2}*x^2\right)} + R_{\min}$$

where x is the distance in inches from the centerline of the foundation tower. $R(x) = 0$ for negative values of x.

The sole testing of walls revealed a similar pattern of diminishing returns. Overall, the moment resistive strength of the walls and anchors combines additively, resulting in a total strength of 96 ft-lbs, giving this foundation design an overall safety factor of 2.1.

ELECTRICAL DESIGN

The turbine electronics convert and optimize power while controlling various subsystems for safe and efficient operation. The entire electrical system was redesigned from previous competition years to promote efficiency and reliability. The turbine electronics are subdivided into four primary segments: rectification, regulation, over-voltage protection, and variable load. The analysis of the turbine control system will conclude with an overview of the assembled hardware. A single-line diagram of the power system can be found in Figure 25.

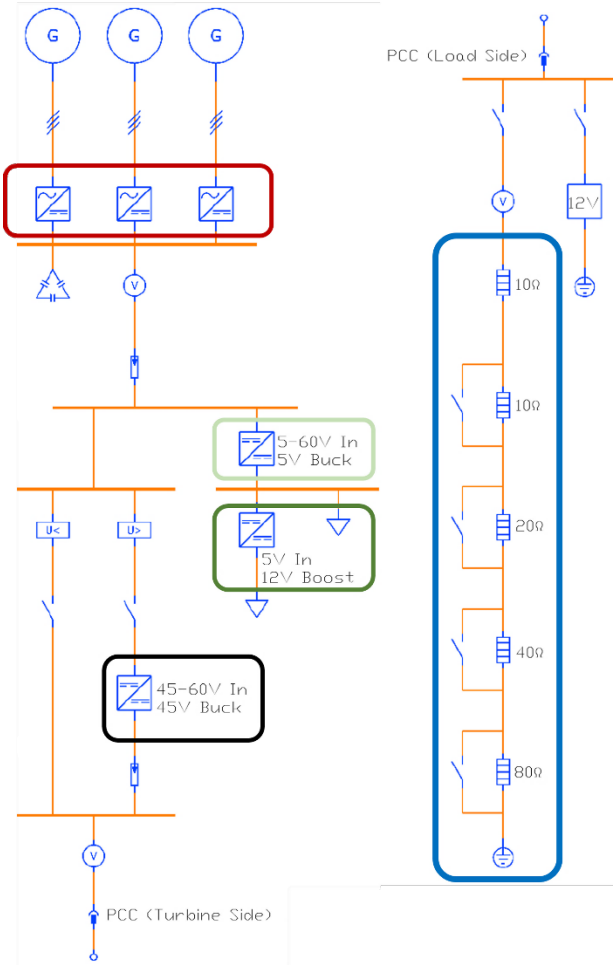

Figure 25 Single Line Diagram (SLD)

Rectification

The generator produces three staggered stages of 3-phase AC power that must be converted to DC power. In previous competition years, the rectification of the nine total AC phases occurred in the turbine electronics box.

In 2022, the team used an 18-24 pin connector to interface the nacelle/tower with the signal modulation circuit box because various sensors were being integrated into the nacelle. It is not feasible to route this many power and signal cables through the tower. Therefore, the team has now moved rectification to the nacelle, which means that we have reduced the number of power connector pins from 9 to 1.

The team has designed an ideal rectifier that uses controller ICs to trigger MOSFETs as switching elements rather than traditional diodes. However, due to the complexity of the circuit, it had to be converted into surface mount components to fit within the size constraints of the nacelle. Because of this, the team went with traditional diode bridge rectifiers this year but plans to introduce ideal rectification in the 2024 competition turbine.

The team is using three FUS45-0045B three-phase bridge rectifiers (boxed in red in Figure 25) because of their low forward voltage drop of 0.55V. To reduce rectification voltage ripple, the team calculated the minimum filtering capacitance using Eq. 6, where N is the generator RPM, P is the number of rotor poles, I is the rectified current, and V_{p-p} is the rectified peak-to-peak voltage ripple.

$$C = \frac{I}{2fV_{p-p}} \; where \; f = \frac{NP}{120} \quad (6)$$

The minimum capacitance was determined to be 1800 µF based on generator RPM values ranging from 0 to 2000 RPM with a desired voltage ripple of 0.1 Vp-p. By mitigating voltage ripple, the turbine will be outputting a cleaner DC voltage thus boosting the power curve score.

Regulation

Certain turbine actuators and sensors require regulated voltage for normal functionality. The power system utilized two primary switching converters boxed in light and dark green within Figure 25. A wide input buck converter operates at an input voltage ranging from 5 to 60 V_{DC}. This converter (shown in light green in Figure 25) converts rectified voltage from the generator to 5 V_{DC} out. 5 V_{DC} is required to power the turbine's two Actuonix L12 actuators, and the A3144 hall effect sensor. A 5V to 12V boost converter (shown in dark green in Figure 25) is connected to the output of the buck converter. It is necessary to have 12V power the turbine's MPXV7002DP pressure differential sensor and two SPDT electromechanical relays. Figure 26 illustrates the schematic of the 5 V_{DC} buck converter based on a TL2575-05 IC. A schematic of the 12 V_{DC} boost converter based on the LM2577-12 IC is found in Figure 27. The maximum current of the buck and boost circuits is 1.2 A_{DC}. Since the primary purpose of the regulation circuits is to power microcontrollers, sensors, and actuators, it will never come close to the maximum current limit.

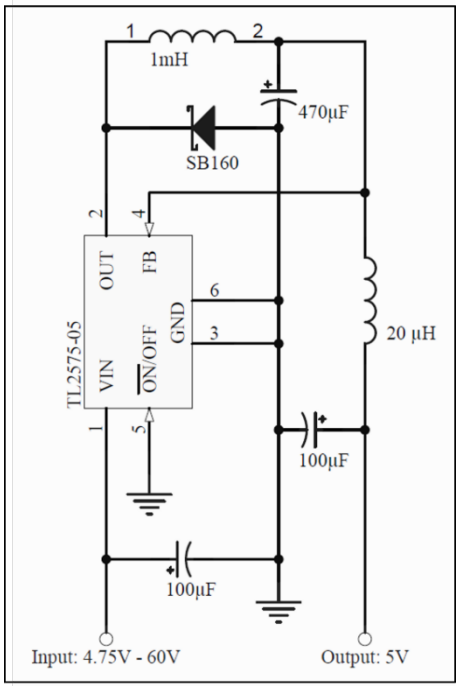

Figure 26 5 V_{DC} Buck Converter

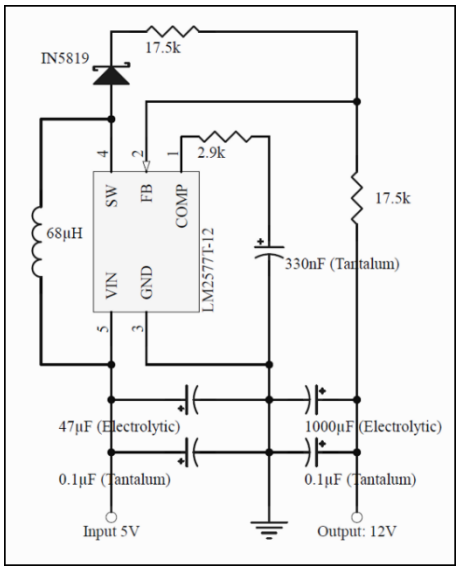

Figure 27 12 V_{DC} Boost Converter

Components for each of the switching converter circuits were chosen with reference to data sheets and predicted performance parameters. Although switching converters are more expensive and complex in comparison to linear regulators, the team chose switching converters due to their high efficiency. As configured, the buck and boost converters in the power system operate at roughly 90% conversion efficiency while linear regulators operate at most 60% efficiency. Switching regulators

also can handle wider input voltage ranges. Buck and boost converters have a high degree of switching noise. To mitigate noise, LC filters are used to smooth out voltage ripples.

PCC Over-voltage Protection

In certain operating conditions, the generator may produce more than 48 V_{DC}. To prevent the PCC voltage from ever exceeding 48 V_{DC}, a third high voltage switching buck circuit based on the LM2576HV is used to limit the turbine's output voltage to 45 V_{DC}. To avoid switching power loss, the over voltage buck circuit will only activate when the PCC voltage sensor reads a value exceeding 45 V_{DC}. Under most operation conditions, the turbine side SPDT relay sends power from the rectifier directly to the PCC thus bypassing the over voltage buck circuit. When the PCC voltage exceeds 45 V_{DC}, the SPDT relay turns on and sends power into the over voltage buck circuit. The turbine power system is designed to withstand at least 60 V_{DC}. If the turbine ever detects generator voltage exceeding 60V, the turbine will shut down. The 45V buck is boxed in black within Figure 25. The schematic of the buck circuit is shown below in Figure 28.

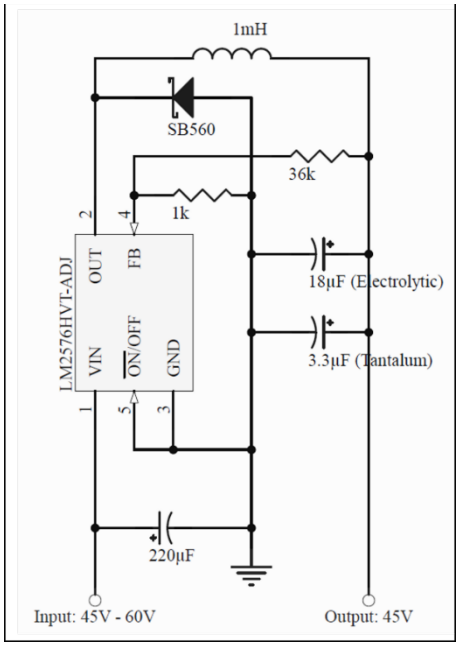

Figure 28 Over Voltage Buck Converter

Load System

As shown in the right side of the SLD (Figure 25). The primary purpose of the load is to power the turbine during startup and dissipate power during normal operation. The load system also houses two microcontroller boards: Arduino Mega 2560 operated by the ATmega2560 chip, and the Arduino Micro operated by the ATmega32U4 chip. The Arduino Mega conducts most of the computation for the control system while the Arduino Micro runs the RPM calculation software.

Variable Load

The variable load is a binary composition of 10 Ω, 20 Ω, 40 Ω, and 80 Ω power resistors in series with a non-controllable 10 Ω resistor as shown in Figure 25 (boxed in blue). SPST relays are connected in parallel to each resistor. When a relay is turned on, current is shorted around the resistor turning it off. This enables the control system to adjust the turbine's load resistance from 10 Ω to 160 Ω in 10 Ω increments.

The team initially tested the variable load with traditional electromechanical relays due to their low cost and availability. The electromechanical relays were prone to failure, and they had a high-power draw. Because of this, searched for solid-state alternatives and chose the newly released IXYS CPC1705Y phototransistor-based solid-state relay. These highly efficient SPST relay ICs utilize p-type optical FETs (normally closed logic) which simplifies the load control software.

When the turbine switches load resistances, there may be millisecond periods where all the controllable resistors are turned off. In these cases, the turbine's load resistance will be 10 Ω because a non-controllable 10 Ω power resistor is always in series with the variable load. This safety feature prevents the turbine load from ever shorting out, which may cause excessive current that could potentially damage the generator or electronics.

Startup Power Source

During startup, the turbine may not be producing enough power to drive all the peripherals. In this condition, the SPDT electromechanical relay sends power from the 12 V_{DC} supply in the load across the PCC into the Turbine. Once the turbine is producing sufficient power, the relay switches on, and power from the generator is sent into the load.

Electromechanical Relay Protection

Within the power system the SPDT relay plays a critical role in directing power in the turbine and in the load. If one SPDT relay fails, the turbine is

unable to function. At the same time, electromechanical SPDT relays are one of the most unreliable parts in the power system. Voltage swings, contact damage, or even physical shock due to travel or drops can break electromechanical relays. Due to the functionality of SPDT relays, there are not many solid-state replacements for SPDT relays. Figure 29 illustrates the SPDT electromechanical relay protection circuit used in both the turbine and load boxes.

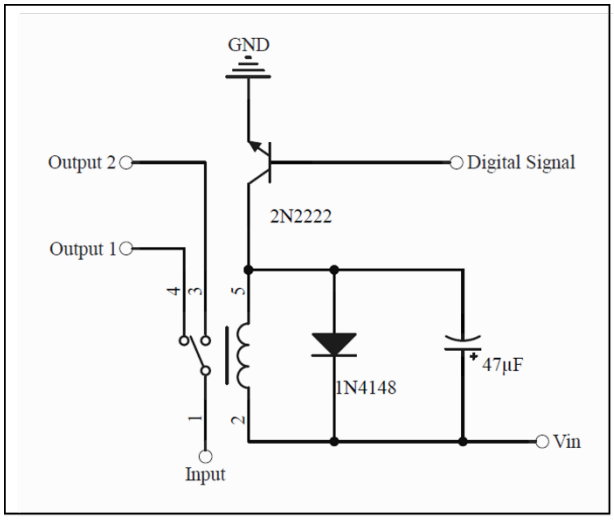

Figure 29 Relay Driving and Protection Circuit

The circuit drives the relay with the 2N2222 BJT which applies just the minimum current to switch on the relay coils. This will prevent over-voltage swings that occur when a relay is switched on and off that can burn out the coil within the relay.

Both the turbine and load circuit boards include custom made sockets to quickly replace the electromechanical relay if it fails. These sockets are made of Dupont female header pins as shown in Figure 30.

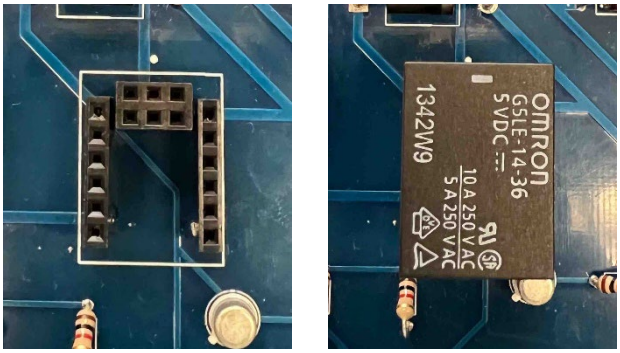

Figure 30 Custom Socket (On Left), Relay Placed into Socket (On Right)

Hardware Overview

The rectification electronics are housed within the Nacelle as shown in Figure 31. A more explicit view of the rectification board can be seen in Figure 32. Nine phases of power from the generator input into the board. The board also supplies GND, 5V, and 12V for the sensors installed inside the nacelle.

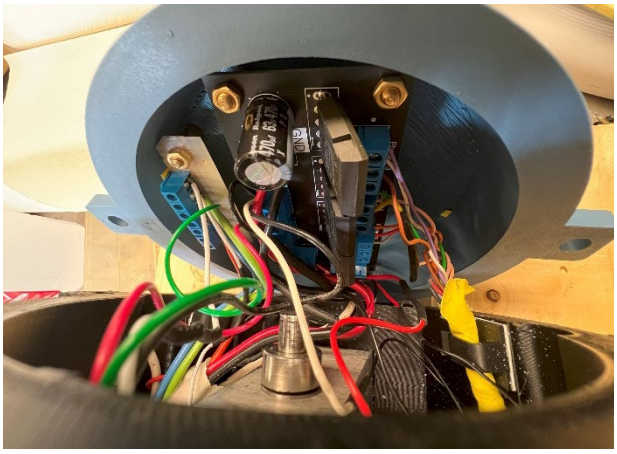

Figure 31 Rectification Board Mounted inside the Nacelle

Figure 32 Rectification Board

A turbine-side Power and Signal Modulation Box houses all the regulators as shown in Figure 33. It also acts as the bus facilitating communication between the load box, and the sensors mounted in the nacelle. The power and signal modulation circuit board can be seen in Figure 34.

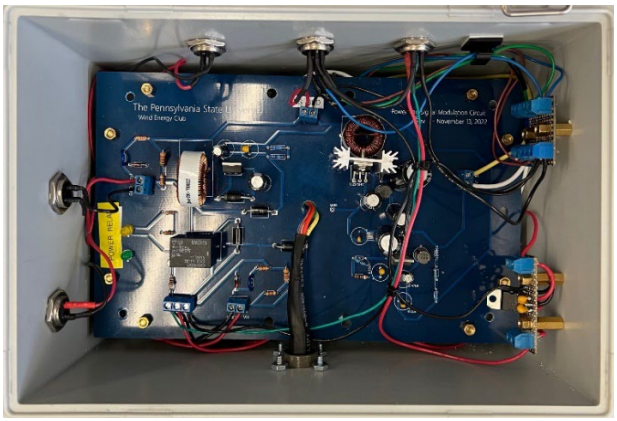

Figure 33 Turbine-Side Power and Signal Modulation Box

The 5V Buck converter is boxed in green, the 12V boost converter is boxed in yellow, the 45V buck converter is boxed in white, and finally the SPDT relay is boxed in red.

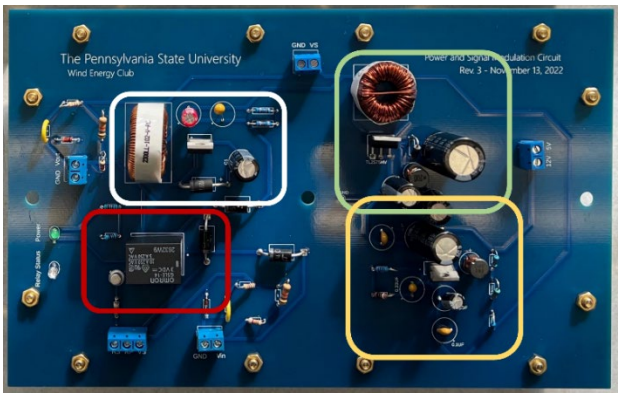

Figure 34 Power and Signal Modulation Board

A Point of Common Coupling (PCC) terminated by Anderson Power Pole connectors facilitates power transmission from the turbine-side Power and Signal Modulation Box to the Load Box. The Load box (shown in Figure 36) houses the variable load circuit and the two microcontrollers.

Figure 35 Variable Load Board

The solid state relays interfacing with the variable load are boxed in white, and the SPDT relay is boxed in red within Figure 35. The load box also uses fans to actively cool the power resistors mounted in the load box.

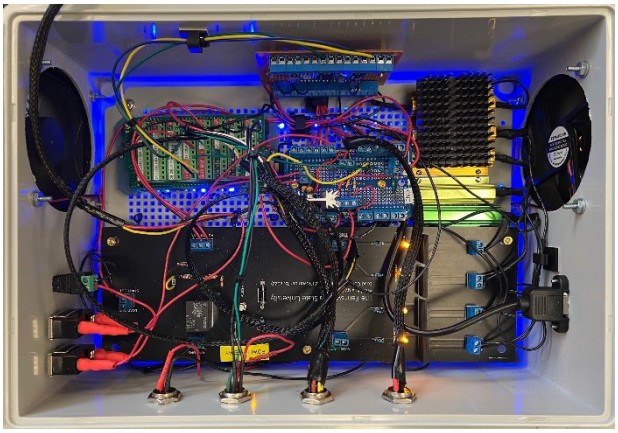

Figure 36 Load Box

Software Design

The objective of the turbine's software is to maintain safety for the turbine while also producing the most power based on the incoming wind speed. The team completely redesigned the turbine control code to address several of the shortcomings experienced during the 2022 competition. There were a lot of shortcomings in last year's code with inefficient data acquisitions and failure to pass safety tasks. For this year, we have implemented many improvements including an efficient codebase, and data collection with visualization capabilities.

State Machine

At the beginning of the semester, the team evaluated several different code architectures. The two major options under consideration were multithreading or state machines. We ultimately decided to design our code as one state machine for its simplicity and efficiency. Due to the nature of embedded systems—which have limited resources—state machines have a much lower memory usage compared to multithreading. State machines can also avoid the overhead of thread management, which requires significantly more resources for memory and processing power to manage and switch between threads. Threading can also create unpredictable execution flow due to thread scheduling and synchronization. State machines allow us to define a clear set of states and transitions between them, giving us predictability and the ability to debug easily.

Each hardware component on the turbine is represented as a module in software. Each module then has a function that represents tasks it should run

during that state. The states are startup, looping, and stop. Using the incoming sensors' values, we determine the state the turbine should be in at any given time. By making each module independent of another, this prevents unintended interactions between the different modules and contributes to a more understandable and maintainable codebase.

Variable Load Control

The load resistance system is created with four resistors of 10, 20, 40, and 80 ohms to generate 16 different possible load resistance through different combinations of each resistor, with an additional 10-ohm resistor to ensure the circuit is not shorted. Given a value to set the system to, we subtract the value by 10 then divide it by 10 to receive a number between 0 - 15. We can then convert this number into its binary representation and set each representing resistor to the value of the binary digit where 1 means on and 0 means off.RPM Sensor

We cannot accurately track RPM on the Arduino Mega that hosts the control code due to the time required to loop through all its processes. The RPM code must loop fast enough to measure the speed of the spinning turbine. Unfortunately, Arduinos can only execute one program at a time, so we implemented an Arduino Micro to separately run the RPM code. The Micro sends data to the Mega through the TX and RX pins using serial communication, while the Mega retrieves the RPM value prompted by the control code.

RPM Sensor

We utilize a hall effect sensor to measure the rotational speed of the generator by detecting changes in a magnetic field caused by the presence of magnets attached to a metal ring in the generator. These magnets are placed near the circumference of the metal ring at opposite ends. When the magnets pass the sensor, they create a magnetic field that causes a voltage drop across the sensor. The frequency of these voltage changes corresponds to the RPM of the generator.

The code that calculates the RPM records the time when it detects a magnet. It saves these times into an array of a size divisible by two; every two magnet detections correspond to one full rotation of the generator. We then take the array and find the latest and earliest times and calculate the difference between the two. Lastly, we use a proportions formula to find the RPM and send this value to the Arduino Mega. Figure 37 compares sensor produced RPM data to dynamometer readouts. The sensor performs very close to the ideal curve shown in green.

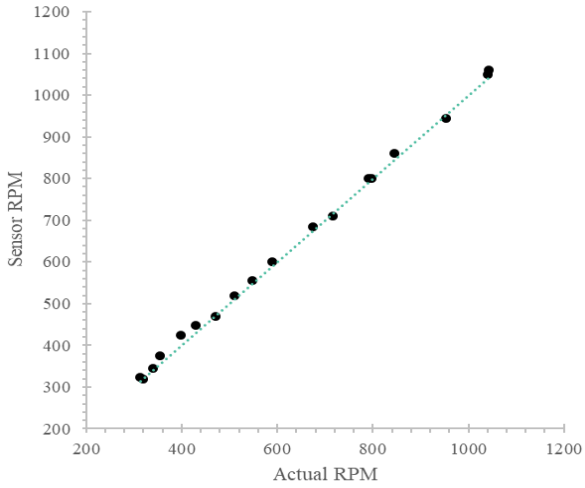

Figure 37 RPM Sensor Performance

Power Curve Task

Power captured by the rotor is obtained via Eq. 7:

$$P_{rotor} = 0.5\rho A v_{wind}^3 C_p \quad (7)$$

where the rotor power coefficient, C_p, is a function of tip speed ratio, λ, and the blade pitch angle, β. A variable load controls the generator's rotational speed, ω_{rotor}, allowing the team to adjust λ because $\lambda = \frac{\omega_{\text{rotor}} R_{\text{rotor}}}{v_{\text{wind}}}$. Controlling λ through the variable load and β with the pitching mechanism, the control system maximizes C_p at any wind speed through a maximum power point tracking (MPPT) algorithm. The turbine's MPPT incremental conductance algorithm measures changes in current, δI, and voltage, δV, to predict how changes in λ or β impact the C_p.

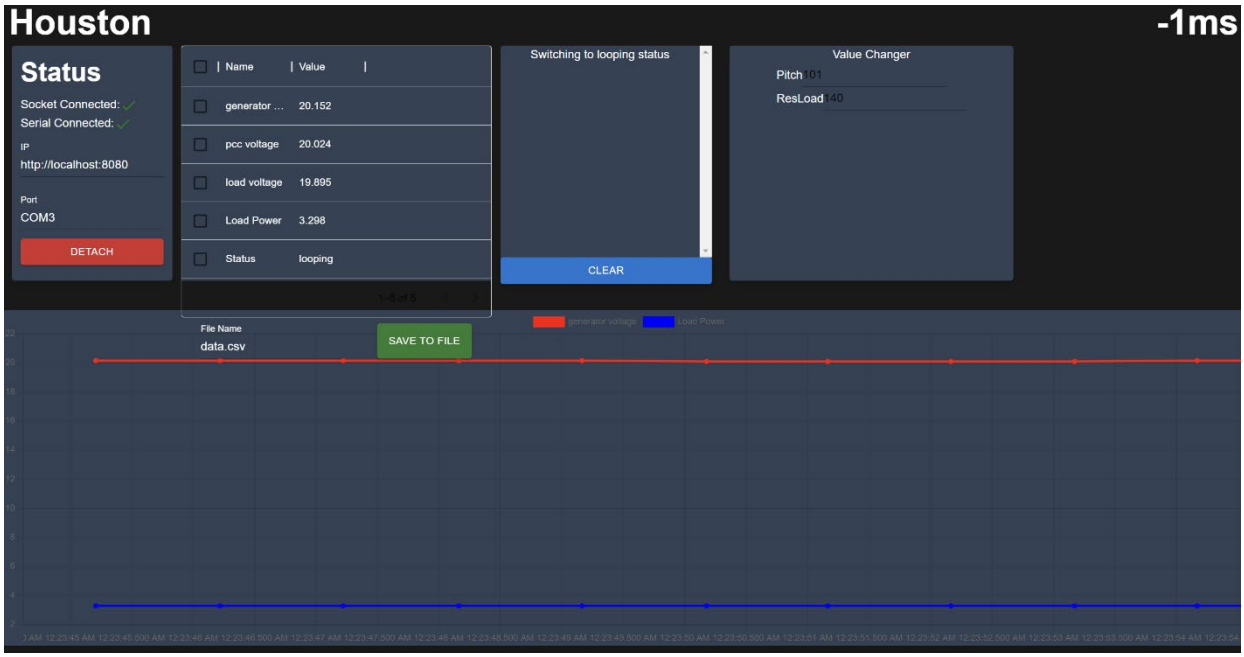

Figure 38 Houston Data Collection

Data Collection Hub

The data collection hub, otherwise known as Houston, is our internal tool for acquiring data and setting parameters on the operating turbine. With Houston, we can display, graph, and save data coming from the Arduino Mega. Houston also allows for live variable tuning during runtime. For example, we can adjust pitch angle to test power production without reuploading code for each test, saving significant testing time. This tool runs on any computer and is very user-friendly. It allows other sub-teams such as Aerodynamics and Electronics to test without having the Software team on hand to individually set testing points. Houston can also automatically save all the experiment data to a .csv file, allowing the other teams to test and acquire data without needing extensive programming experience.

Deep Dive into States

Startup Mode – In startup, we will initialize sensors, the wind turbine will pitch to its starting angle, and check for PCC disconnect or emergency stop. If either is detected, it will move to stop. If not, it will keep repeating these operations until we detect over 9 volts in the generator, then it will move to the looping state.

Looping – In looping, the wind turbine will detect if we are in power curve, rotor speed control, or durability test base on the wind speed. The wind turbine will then try to find the best pitch angle and load resistance to accomplish the needed goal. To learn how we do this, please refer to the interpolation section. If the load voltage ever exceeds 45 volts, power is redirected through the 45-volt buck circuit to reduce the output voltage to meet competition standards. On top of this, the turbine is also constantly checking if the emergency stop has been pressed or if there is a PCC disconnect. If either an

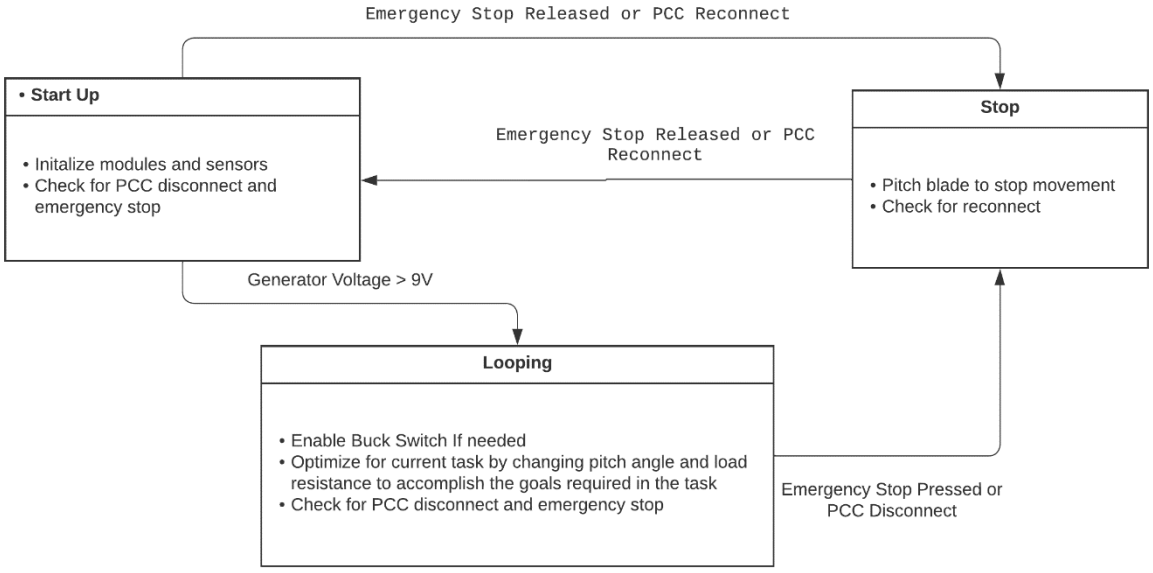

Figure 39 Emergency Stop/PCC Disconnect

emergency stop or PCC disconnect has been detected, we move to the stop switch.

Stop – In stop, the turbine will pitch to a predetermined angle that we know will stop the blades from spinning and maintain it. It will also check if we can move back to startup. If the stop state was caused by the emergency stop button, it will simply move back to startup once the button has been released. If it is a PCC disconnect, then we first wait for the voltage in the PCC to drop below a certain threshold. This means we have truly stopped the blades and prevented false startups. Then we wait for the PCC voltage to go above a threshold to move to the startup state.

Interpolation

Interpolation – If a data set is nonlinear, then a linear regression would obviously be a poor choice. Not only would it be inaccurate, but there would also be points of discontinuity. However, by using cubic spline interpolation, a smooth curve can be generated between each pair of points. Overall, this would create a continuous curve that provides a smooth estimate of data while minimizing the error between the curve and the data points. It is also very light on computation since the cubic spline function is generated beforehand, so the actual interpolation during runtime is simply a few multiplications.

TURBINE TESTING

XTURB-PSU Simulation models produced the data illustrated in Figure 40. At start-up and low wind speeds, high pitch angles must be used to achieve the most optimal C_P (power coefficient). As the wind speed increases, pitch angles must be reduced to achieve the highest C_P. The most optimal rotor power coefficient is achieved at a pitch angle of 1.5 degrees and a TSR of 4.1.

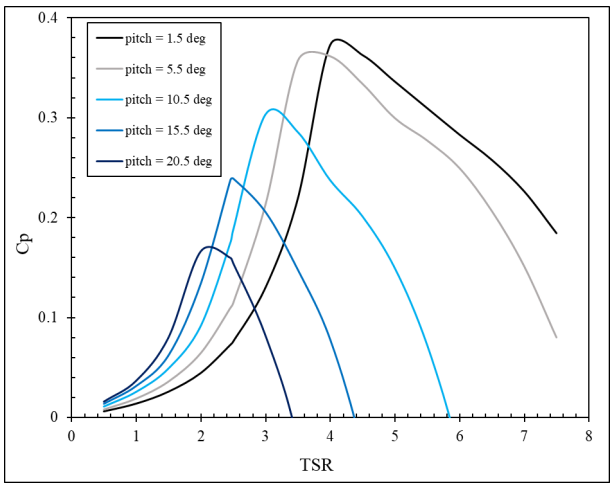

Figure 40 C_p versus λ

The team was only able to reserve one week of wind tunnel testing prior to the submission of the deliverable. It was soon discovered that the pitching mechanism was configured to pitch from 0° to -8°; however, the airfoils were only designed to function optimally in positive pitch range from 1.5° to 55°. Because of this, sub-optimal power curves were obtained through testing as shown in Figure 41 and Figure 42. The team has readjusted the pitching mechanism so that it can now pitch through 0° to 50°, so that proper experimental Cp/λ curves will be ready for the Q/A session.

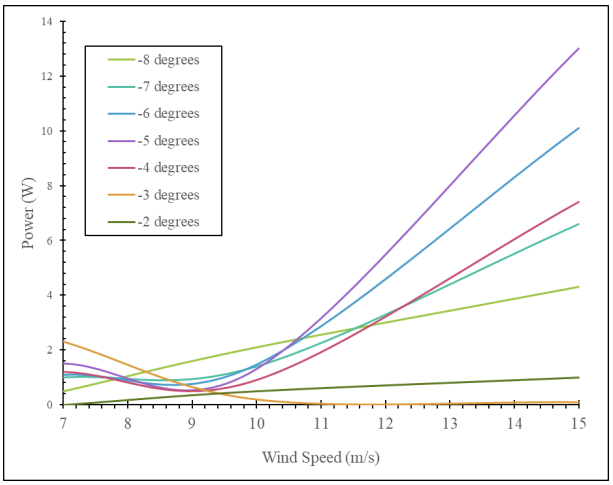

Figure 41Power Output with Negative Pitch at 80 Ω

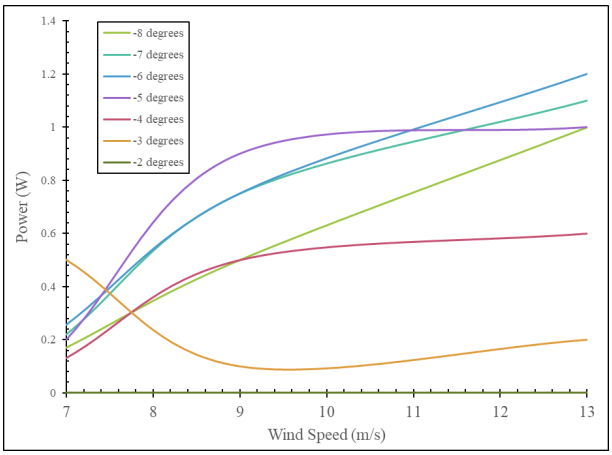

Figure 42 Power Output with Negative Pitch at 120 Ω

COMMISSIONING CHECKLIST

Table 1 displays a checklist utilized to confirm that the turbine is free from any damage, assembled accurately, and functioning normally.

Table 1: Commissioning Checklist

Turbine Testing Verification Procedure	Team Lead #1 Certification	Team Lead #2 Certification
Generator Subsystem Verification Steps		
Check for damage or cracks to the generator stators		
Confirm 3-Phases are connected to each of the three stages		
Tighten the set screws on the rotors		
Confirm airgap between every rotor and stator		
Verify signal and power cables are not in contact with the rotors		
Aerodynamic Subsystem Verification Steps		
Verify the servos are attached properly to the nacelle		
Tighten all fasteners in the pitch mechanism		
Confirm that the mechanism is not locked up		
make sure the 7-pin connector cable is connected properly to the electronics/sensors in nacelle		
Check blade for structural integrity		
Attach blades to pitching mechanism		
Attach nacelle lid to the nacelle middle piece		
Electronics Subsystem Verification Steps		
attach the 7-line cable to the turbine box		
Connect communication cables between load and turbine box		
Connect E-stop out wire to the emergency stop button		
Connect PCC cables from both load and turbine box to wind tunnels connectors		
Plug in the 12v input on the load box and flip the switches on		
Check all indication lights for power (Relay, Arduino, Load)		
Foundation Subsystem Verification Steps		
Ensure foundation walls are unbent		
Ensure foundation walls are slotted together fully		
Tighten angle brackets to walls with washer		
Tighten walls to top plate		
Pull wires through foundation tower		
Secure foundation tower to top plate		
Final Verification Steps		
Connect 7-line cable from nacelle to 7-line cable from foundation power		
Line up flange holes with studs on transition piece and place turbine on top		
Ensure the turbine is facing the correct direction		

ANNUAL ENERGY PRODUCTION

A Weibull distribution was applied to the simulated turbine power curve to estimate annual energy production. Figure 43 shows the input power curve used based on XTURB-PSU simulation data. Figure 44 illustrates the output annual energy production for average annual wind speeds ranging from 3 m/s to 8m/s.

The scale factor of the Weibull distribution (λ) is determined through Eq. 8:

$$\lambda = \frac{\bar{u}}{\left(\frac{\sqrt{\pi}}{2}\right)} \qquad (8)$$

Where, $\bar{u}$ is the annual average wind speed and the shape factor, k, is set to 2 (Rayleigh distribution). The Weibull values as set by these parameters were multiplied by the wattage of the power curve and the number of hours in a year. The sum of these values provided the energy production for a particular annual average wind speed condition as shown in Figure 44.

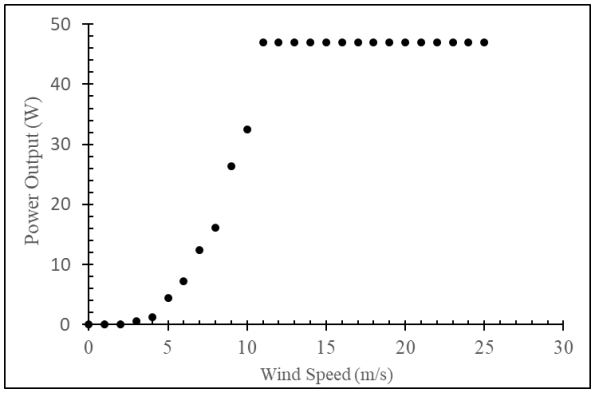

Figure 43 Turbine Power Curve

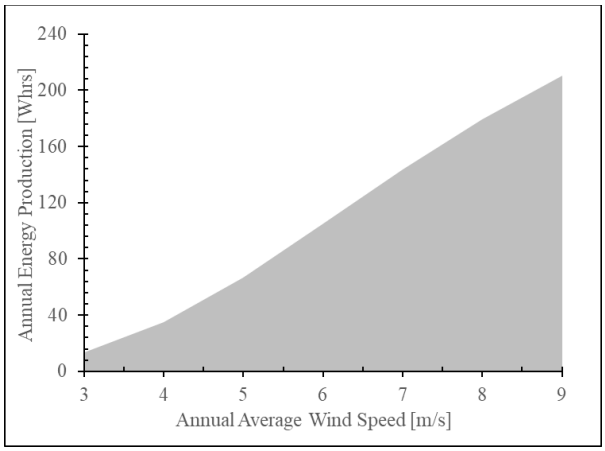

Figure 44 Annual Energy Production vs Annual Average Wind Speed

DESIGN CHANGES TABLE

AEROSPACE SUBSYSTEM	
Nacelle	A new bottle-shaped nacelle was designed for the 2023 competition year
Blades	New blade material (Rigid 10K) Same blade design as 2021
Pitching Mechanism	A new linear actuator-based pitching mechanism was designed and moved to the inside of the Nacelle
Fins	New "Tie-fighter" like blades were designed for the turbine
GENERATOR SUBSYSTEM	
Rotors	New rotors were designed and built to replace the old rotors from 2018
Stators	The same stator design from 2018 is still being used in the 2023 competition
ELECTRICAL SUBSYSTEM	
Rectifier Board	A new rectifier board was designed and mounted to the nacelle
Turbine box	A new turbine box was designed and built with a custom power and signal modulation circuit board
ELECTRICAL SUBSYSTEM CONTINUED	
Load Box	A new turbine box was designed and built with a custom variable load circuit board
FOUNDATION SUBSYSTEM	
Foundation	The entire foundation sand screw egg foundation is newly designed and built
SOFTWARE SUBSYSTEM	
Turbine Code	The entire turbine code was written from scratch
Houston DAQ	The Houston Data Collection hub was newly designed for the 2023 competition

References

[1] “Rigid 10K,” *RIGID 10K MATERIAL PROPERTIES DATA*. [Online]. Available: https://asset.dynamism.com/media/catalog/product/pdf/Formlabs_Rigid_10K_TDS.pdf. [Accessed: 04-May-2023].

[2] C. Chen, T. Wang, and L. Wang, “Sensitivity study of the influence of blade sectional stiffness parameters on the aeroelastic response of wind turbines,” *Frontiers*, 21-Jun-2021. [Online]. Available: https://www.frontiersin.org/articles/10.3389/fenrg.2021.707082/full. [Accessed: 04-May-2023].

[3] “Linear Regulator and switching regulator (what is the difference between linear and switching regulators?),” *ROHM*. [Online]. Available: https://www.rohm.com/electronics-basics/dc-dc-converters/linear-vs-switching-regulators. [Accessed: 04-May-2023].

[4] “Magnetism Basics,” *How magnets work*. [Online]. Available: https://ece.northeastern.edu/fac-ece/nian/mom/work.html. [Accessed: 10-Feb-2022].

[5] S. Fahey, “Basic Principles Of The Homemade Axial Flux Alternator Basic Principles Of The Homemade Axial Flux Alternator,” Dec. 2016.

[6] K. C. Latoufis, G. M. Messinis, P. C. Kotsampopoulos, and N. D. Hatziargyriou, “Axial Flux Permanent Magnet Generator design for low cost manufacturing of small wind turbines,” *Wind Engineering*, vol. 36, no. 4, pp. 411–431, 2012.

[7] “The K&J Magnetic Field Calculator,” *K&J Magnetics*. [Online]. Available: https://www.kjmagnetics.com/fieldcalculatorold.asp. [Accessed: 04-May-2023].